A fast method for retrieval of cloud parameters using oxygen A-band measurements from the Global Ozone Monitoring Experiment.

Koelemeijer, R.B.A.; Stammes, P.; Hovenier, J.W.; de Haan, J.F.

published in
Journal of Geophysical Research. Atmospheres
2001

DOI (link to publisher)
10.1029/2000JD900657

document version
Publisher's PDF, also known as Version of record

JOURNAL OF GEOPHYSICAL RESEARCH, VOL. 106, NO. D4, PAGES 3475–3490, FEBRUARY 27, 2001

A fast method for retrieval of cloud parameters using oxygen A band measurements from the Global Ozone Monitoring Experiment

R. B. A. Koelemeijer and P. Stammes

Royal Netherlands Meteorological Institute, De Bilt, Netherlands

J. W. Hovenier[1] and J. F. de Haan[2]

Department of Physics and Astronomy, Free University, Amsterdam, Netherlands

Abstract. The Global Ozone Monitoring Experiment (GOME) on board the ERS-2 is designed to measure trace gas column densities in the Earth's atmosphere. Such retrievals are hindered by the presence of clouds. The most important cloud parameters that are needed to correct trace gas column density retrievals for the disturbing effects of clouds are the (effective) cloud fraction and cloud top pressure. At present, in the operational GOME data processor an effective cloud fraction is derived for each pixel, but cloud top pressure is assumed a priori and is deduced from a climatological database. Here we report an improved cloud retrieval scheme, which simultaneously retrieves the effective cloud fraction and cloud top pressure from GOME data. This algorithm, called Fast Retrieval Scheme for Clouds from the Oxygen A band (FRESCO), makes use of reflectivities as measured by GOME inside and outside the oxygen A band (758–778 nm). For validation, the results of FRESCO are compared to effective cloud fractions and cloud top pressures derived with standard methods from colocated measurements made by the Along Track Scanning Radiometer-2 (ATSR-2). The brightness temperatures of the cloudy pixels as measured by ATSR-2 are related to cloud top pressures using temperature profiles from the European Center for Medium-range Weather Forecasts model. Generally, the results from FRESCO and ATSR-2 agree reasonably well. For the effective cloud fractions the average difference (based on a comparison of 322 points) is 0.04; the standard deviation is 0.09. For the cloud top pressures, only points with an effective cloud fraction larger than 0.1 have been compared. For these 236 points the average difference in cloud top pressure is 65 hPa, and the standard deviation is 92 hPa.

1. Introduction

The Global Ozone Monitoring Experiment (GOME) on board the ERS-2 satellite of the European Space Agency, is a four-channel grating spectrometer measuring the Earth's reflectivity between 237 and 794 nm, with a spectral resolution of 0.2–0.4 nm. The pixel size of GOME can be varied but is often 40 × 80 km^2 or 40 × 320 km^2. The primary geophysical product of GOME is the ozone vertical column density. Other trace gas column densities retrieved from GOME measurements are NO_2 (operational) and, for specific observation conditions, trace gases such as BrO, SO_2, and OClO [*Burrows et al.*, 1999, and references therein]. Since clouds are one of the largest error sources in trace gas column density retrievals from ultraviolet and visible reflectivities, the presence of clouds should be taken into account in such retrievals. Therefore, as part of the operational GOME ozone column density retrieval algorithm, cloud fraction is derived by the Initial Cloud Fitting Algorithm (ICFA) [*Deutsches Zentrum für Luft- und Raumfahrt (DLR)*, 1994]. This algorithm is based on the work of *Kuze and Chance* [1994] and consists of chi-square minimization of a measured and a simulated spectrum from 758 to 778 nm (enclosing the O_2 A band), thereby solving for the cloud fraction. Cloud top pressure, however, is assumed a priori and is taken from the International Satellite Cloud Climatology Project

[1] Also at Astronomical Institute "Anton Pannekoek", University of Amsterdam, Amsterdam, Netherlands.

[2] Also at Royal Netherlands Meteorological Institute, De Bilt, Netherlands.

Paper number 2000JD900657.
0148-0227/01/2000JD900657$09.00

(ISCCP) database [*Rossow and Garder,* 1993]. However, the actual cloud top pressure may be very different from the climatological mean value. An error in the assumed cloud top pressure leads to an error in the cloud fraction and surface albedo value derived using ICFA [*Koelemeijer and Stammes,* 1999a]. The long-term goal of our investigations is to improve the correction for cloud effects in the retrieval of vertical column densities of ozone and other trace gases. For that purpose, we developed a method in which both cloud fraction and cloud top pressure are derived from the O_2 A band. This method, called Fast Retrieval Scheme for Clouds from the Oxygen A band (FRESCO), is computationally efficient such that it is suitable for application in near-real-time retrievals of ozone column densities.

Besides the O_2 A band method, discussed below, a number of other methods have been used to determine cloud top pressure or height from space. A few experiments have been performed with active instruments, such as the Lidar In Space Technology Experiment (LITE) [*Winker and Trepte,* 1998]. Most often, however, passive techniques have been used. The so-called brightness temperature method is frequently used to derive cloud top pressure [e.g., *Stowe et al.,* 1988; *Rossow and Garder,* 1993]. This method is used here as well to derive cloud top pressures from Along Track Scanning Radiometer-2 (ATSR-2) measurements, to which we compare our FRESCO results. Another method employing thermal infrared radiance measurements is the CO_2 slicing method, pioneered by *Smith and Platt* [1978]. Stereoscopy was used by *Prata and Turner* [1997] to determine cloud top height from near-infrared and thermal infrared radiances, exploiting the dual-view capability of the ATSR. However, its accuracy is limited to ~1 km, owing to cloud motion in the time between nadir and forward view acquisition, and is limited to clouds with distinctive spatial structures. *Joiner and Bhartia* [1995] used the Ring effect in the ultraviolet, due to rotational Raman scattering, to derive cloud top pressures from Total Ozone Mapping Spectrometer (TOMS) measurements. These pressures were compared to cloud top pressures derived from Temperature Humidity Infrared (THIR) sounder brightness temperature measurements. As a result, a standard deviation of 257 hPa between cloud top pressures derived from TOMS and THIR was obtained for scenes with a reflectivity larger than 0.7; the difference is attributable to the TOMS spectral resolution and the accuracy of the THIR cloud top pressures. Recently, *Knibbe et al.* [2000] used the GOME polarization measurements in the ultraviolet and visible to determine cloud top pressures from GOME data for scattering angles near 90°. They estimated the accuracy of the cloud top pressures derived from the GOME polarization measurements to be ~150 hPa, mainly due to measurement uncertainties.

Retrieval of cloud top pressure from the oxygen A band has a long history beginning with the first suggestions by *Yamamoto and Wark* [1961] and *Chapman* [1962]. The first satellite measurements were made from Gemini-5 in August 1965 [*Saiedy et al.,* 1967]. Investigations on the theoretical side were made by, among others, *Wu* [1985], who studied to some extent the impact of multiple scattering inside clouds on retrievals of cloud top pressure from O_2 A band measurements; by *Fischer and Grassl* [1991], who performed a detailed sensitivity study for cloud top pressure retrieval; and by *O'Brien and Mitchell* [1992], who studied the influence of instrumental error sources and retrieval assumptions on the accuracy of O_2 A band derived cloud top pressures, but only for optically thick clouds with a cloud fraction of 1. *O'Brien and Mitchell* [1992] give a fairly detailed overview of the work on cloud top pressure retrieval from the O_2 A band, up to 1992. *Fischer et al.* [1991] applied their retrieval method to airborne O_2 A band measurements, showing good agreement with lidar determinations of cloud top altitude. With the launch of the satellite instruments GOME (operational from April 1995 till present) and POLDER (operational from August 1996 till June 1997), the first routine space-based measurements of the reflected radiation in the O_2 A band have become available. Recently, *Vanbauce et al.* [1998] used the POLDER measurements to derive apparent pressures above ocean, which can be used for cloud detection by comparing the apparent pressures to the expected surface pressure.

The aim of this paper is to present the FRESCO algorithm in detail, together with a sensitivity analysis and a validation using colocated ATSR-2 data. The paper is structured as follows. In section 2 the FRESCO retrieval method is described. A study of the influence of several model assumptions and measurement errors on the retrieved cloud fraction and cloud top pressure is presented in section 3. Section 4 deals with the method to derive cloud fraction and cloud top pressure from ATSR-2 measurements. In section 5 a comparison is made between FRESCO and ATSR-2 cloud fractions and cloud top pressures. The differences in the retrieved cloud top pressures between FRESCO and ATSR-2 are discussed in section 6. Conclusions are presented in section 7.

2. Data and Retrieval Method

2.1. GOME Data

The GOME instrument measures the Earth's reflected radiance and the solar irradiance at wavelengths between 237 and 794 nm. The light entering the instrument is dispersed using a predisperser prism and four gratings (one grating for each optical channel), after which it is recorded by four diode-array detectors with 1024 detector pixels each. In FRESCO we make use of the GOME measurements between 758 and 766 nm, which are in GOME channel 4. The spectral resolution of GOME is determined by the slit function. This function has been measured prelaunch and can be repre-

sented by the following functional form [*European Space Agency (ESA)*, 1996]:

$$f(\lambda'-\lambda)=\frac{a_1}{(\lambda'-\lambda)^2+a_2}+\frac{a_3}{(\lambda'-\lambda)^4+a_4}+\frac{a_5}{(\lambda'-\lambda)^6+a_6}, \quad (1)$$

where for the wavelengths considered, $a_1=6.234\times10^{-4}$ nm, $a_2=2.307\times10^{-2}$ nm^2, $a_3=1.029\times10^{-3}$ nm^3, $a_4=9.895\times10^{-4}$ nm^4, $a_5=6.268\times10^{-5}$ nm^5, $a_6=4.244\times10^{-5}$ nm^6, and $\lambda'-\lambda$ is the spectral distance (in nm) from the central position of the detector pixel at wavelength λ. The full width at half maximum (FWHM) is 0.367 nm for the wavelengths considered. Using GOME in-flight measurements, *Caspar and Chance* [1997] independently determined the FWHM to be 0.35 ±0.02 nm. The spectral sampling distance of GOME is 0.207 nm in this spectral region. The slit function is normalized according to

$$\int_0^\infty f(\lambda'-\lambda)\,d\lambda'=1. \quad (2)$$

The radiance measured by GOME, $\bar{I}(\lambda)$, is hence given by

$$\bar{I}(\lambda)=\int_0^\infty f(\lambda'-\lambda)\,I(\lambda')\,d\lambda', \quad (3)$$

where $I(\lambda')$ is the monochromatic radiance of the Earth. An analogous equation holds for the measured solar irradiance perpendicular to the beam, $\pi\bar{F}_0(\lambda)$. The Earth's reflectivity at the top of the atmosphere, $R_{\text{meas}}(\lambda)$, is obtained from

$$R_{\text{meas}}(\lambda)=\frac{\bar{I}(\lambda)}{\cos\theta_0\,\bar{F}_0(\lambda)}, \quad (4)$$

in which θ_0 is the solar zenith angle.

2.2. Retrieval Method

2.2.1. Principle. The principle of the FRESCO retrieval algorithm is explained by referring to Figure 1, which shows O_2 A band measurements for two cloudy pixels over Scotland, measured by GOME on July 23, 1995, 1151 UT. From weather maps and the corresponding ATSR-2 image we know that the clouds belong to a cold front pertaining to a low-pressure area with its center north of Scotland. One pixel is in the center of the frontal zone and contains mainly high clouds, and one pixel is in the cold area behind the front and contains mainly low clouds. Figure 1 shows their normalized reflectivity spectra in and around the O_2 A band. The reflectivities in Figure 1 have been normalized by their continuum value at 758 nm, where no absorption occurs. These continuum reflectivities are 0.789 for the high cloud and 0.681 for the low cloud. The decrease in reflectivity with respect to the continuum value due to absorption by oxygen can be observed clearly in these spectra. The reflectivity in the continuum is mainly determined by the cloud fraction, the cloud optical thickness (or cloud albedo), and the surface albedo. Inside the O_2 A band, however, the reflectivity depends on the cloud top pressure as well because clouds screen nearly all the oxygen below them and, to a lesser extent, inside them. Therefore the O_2 A band is deeper for the pixel with the low cloud than for the pixel with the high cloud. Combined information on cloud fraction and cloud optical thickness may, in principle, be derived from the reflectivity in the continuum, whereas the cloud top pressure can be inferred from the depth of the O_2 A band, as oxygen is a well-mixed gas.

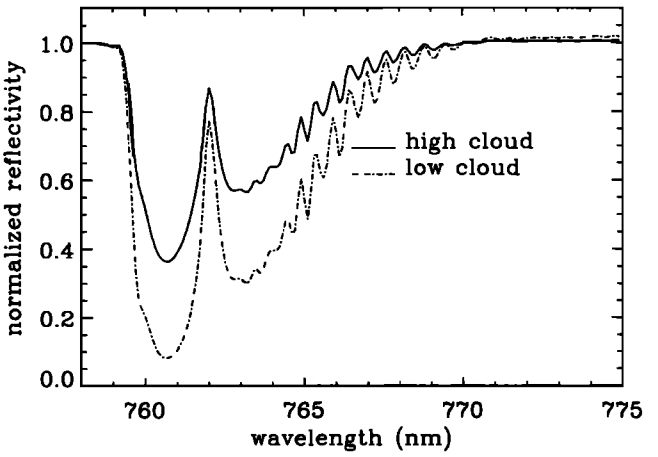

Figure 1. Example of GOME measurements of the oxygen A band. The reflectivity spectra are normalized to unity at 758 nm. The high-cloud and low-cloud pixels have comparable illumination and viewing directions. The spectral resolution of GOME at these wavelengths is ~0.36 nm; the spectral sampling is ~0.207 nm.

2.2.2. Method description. In FRESCO, three ~1-nm-wide wavelength windows are used, namely, 758–759 nm (continuum, no absorption), 760–761 nm (strong absorption), and 765–766 nm (moderate absorption). Each window comprises five GOME wavelengths. It is important to note that the reflectivities in these three wavelength windows contain nearly all independent information that is available in the O_2 A band for instruments with the spectral resolution of GOME [*Kollewe et al.*, 1992]. The FRESCO retrieval method is based on comparing the measured and simulated reflectivities in these three wavelength windows.

To simulate the spectrum of a (partly) cloudy GOME pixel, some assumptions are made in FRESCO (see Figure 2). A pixel is assumed to consist of a clear and a cloudy part, with a fractional area of $(1-c)$ and c, respectively, where c is the cloud fraction. We assume that the contributions of the clear and cloudy parts of the pixel to the reflectivity at the top of the atmosphere can be written as the sum of the reflectivities of a completely clear and a completely cloudy pixel weighted with the cloud fraction; that is, adjacency effects are neglected. To simplify the retrieval, molecular scattering, scattering and absorption by aerosols, and absorption by oxygen inside and below the cloud are

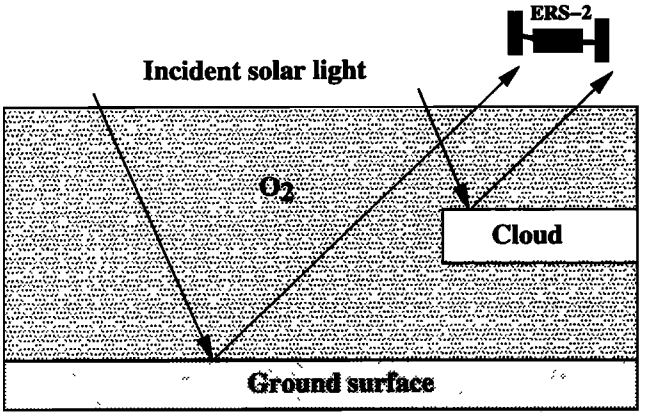

Figure 2. The two types of photon paths used in the FRESCO retrieval algorithm to simulate the spectrum of a partly cloudy pixel.

neglected. Only absorption due to oxygen above the cloud or ground surface is taken into account, as well as reflection by the cloud top or surface, both of which are assumed to be Lambertian reflectors. We refer to this model as a bireflector model, in which two types of photon paths through the atmosphere to the detector are possible: (1) from the Sun to the ground surface and then to the satellite and (2) from the Sun to the cloud top and then to the satellite. Along these paths, shown in Figure 2, attenuation occurs because of absorption by oxygen.

We now consider this attenuation process in our model. For a plane-parallel atmospheric layer the slant path factor, defined as the ratio of the path traveled by a beam of photons incident on that layer under a zenith angle ξ to its geometrical thickness, is given by $s_{\rm pp}(\xi) = 1/\cos\xi$. The angle ξ is equal to the solar zenith angle at the surface, θ_0, or the viewing zenith angle at the surface, θ. In our model we take into account the Earth's sphericity to calculate the photon path. The slant path factor for an atmospheric layer between height z and $z+dz$ in a spherical atmosphere is given by

$$s_{\rm sp}(\xi, h) = \frac{h + R_*}{\sqrt{R_*^2 \cos^2\xi + h^2 + 2R_* h}}, \qquad (5)$$

where R_* is the sum of Earth's radius and the height of the reflecting surface above the ground, z_r, and $h = z - z_r$ is the height of the atmospheric layer above the reflecting surface [cf. *Sarkissian et al.*, 1995]. For a spherical atmosphere the total slant path factor of the atmosphere, $s_{\rm tot,sp}$, is the integral of $s_{\rm sp}$ over height, weighted with the oxygen number density $n_{\rm o_2}$ according to

$$s_{\rm tot,sp}(\xi) = \frac{\int_0^\infty n_{\rm o_2}(z) s_{\rm sp}(\xi, z) dz}{\int_0^\infty n_{\rm o_2}(z) dz}. \qquad (6)$$

Obviously, for a plane-parallel atmosphere the total slant path factor is $s_{\rm tot,pp}(\xi) = s_{\rm pp}(\xi)$. Assuming a midlatitude summer atmosphere [*Anderson et al.*, 1986], the relative difference in $s_{\rm tot}$ between a plane-parallel and a spherical atmosphere, defined as $(s_{\rm tot,pp} - s_{\rm tot,sp})/s_{\rm tot,sp}$, is smaller than 1% for $\xi \leq 70°$; for ξ=75° it is 1.6%; for ξ=80° it is 3.7%; and for ξ=85° it increases to 13%. We note that these numbers agree well with the values of the Chapman function, reported by *Van de Hulst* [1980, p. 667]. The attenuation of light, transmitted through the atmosphere from the top of the atmosphere to an altitude z_r and then to the satellite, is determined by the slant oxygen optical thickness, $b^{sl}_{\rm o_2}(\lambda', z_r, \theta, \theta_0)$ and is equal to

$$\int_{z_r}^\infty \sigma_{\rm o_2}(\lambda', z) n_{\rm o_2}(z) [s_{\rm sp}(\theta_0, z - z_r) + s_{\rm sp}(\theta, z - z_r)] dz, \quad (7)$$

where $\sigma_{\rm o_2}(\lambda', z)$ is the oxygen absorption cross section. The transmittance $T(\lambda')$ along the photon paths of our model at wavelength λ' is then given by

$$T(\lambda', z_r, \theta, \theta_0) = e^{-b^{sl}_{\rm o_2}(\lambda', z_r, \theta, \theta_0)}. \qquad (8)$$

Since the O_2 absorption cross section depends strongly on wavelength, line-by-line transmittances $T(\lambda', z_r, \theta, \theta_0)$ were calculated using the high resolution transmission molecular absorption database HITRAN'96 [*Gamache et al.*, 1998]. For our calculations the pressure and temperature profiles have been taken from the midlatitude summer atmosphere. The line-by-line transmittances have been convoluted with the GOME slit function, analogous to (3), to yield the convoluted transmittance $\bar{T}(\lambda, z_r, \theta, \theta_0)$. The convoluted transmittances have been stored in a database as a function of λ, θ, θ_0, and the pressure P corresponding to altitude z_r.

According to our bireflector model the simulated reflectivity $R_{\rm sim}(\lambda)$ can now be written as

$$\begin{aligned} R_{\rm sim}(\lambda) &= (1-c)\, A_s\, \bar{T}(\lambda, P_s, \theta, \theta_0) \\ &+ c\, A_c\, \bar{T}(\lambda, P_c, \theta, \theta_0), \end{aligned} \qquad (9)$$

where A_s and A_c are the surface and cloud albedo, respectively, and are assumed to be independent of wavelength in the range concerned; P_s and P_c are the pressures at the ground surface and cloud top, respectively.

By assuming values for P_s, A_s, and A_c the cloud fraction and cloud top pressure are derived by nonlinear least squares minimization of the difference between the measured spectrum $R_{\rm meas}(\lambda)$ and the simulated spectrum $R_{\rm sim}(\lambda)$ and varying c and P_c. For this minimization we make use of the Levenberg-Marquardt method [*Press et al.*, 1986]. The reflectivities at the different wavelengths have been given the same weight in the minimization. For the solution (c, P_c) we have $R_{\rm sim}(\lambda) \approx R_{\rm meas}(\lambda)$ for all wavelengths. We assume for the sea surface pressure a constant value of 1013 hPa; for land we account for the elevation of the ground surface, which is deduced from the ETOPO5 database. The albedo of sea is taken to be 0.02, and the albedo of land is deduced from a global minimum-reflectivity database, which we composed for this purpose using two

months of GOME data (a July and a January month). We interpret these minimum-reflectivity data as Lambertian surface albedos. The spatial resolution of this surface albedo database is 2.5° × 2.5°. Generally, it is not feasible to derive cloud fraction and cloud optical thickness (or cloud albedo) independently from the GOME data (see section 2.2.3). Therefore, in addition to cloud top pressure, here as well as in ICFA, only an "effective" cloud fraction is derived, which is the derived cloud fraction assuming an a priori chosen cloud optical thickness or cloud albedo. In the remainder of this paper we assume a cloud albedo of 0.8, unless specified otherwise, and use the term effective cloud fraction for c. In section 2.2.3 we will discuss the validity of using an effective cloud fraction, and we will motivate our choice A_c=0.8, which corresponds to an optically thick cloud.

2.2.3. Concept of effective cloud fraction. In operational meteorology, cloud fraction is understood to be the fractional coverage of the sky by clouds. Traditionally, this is reported by observers at meteorological stations and is expressed in octas (multiples of 1/8th). The reported cloud fraction is independent of the cloud optical thickness, provided that the cloud is optically thick enough to be detected by the human eye. However, in the case of GOME it is impossible to uniquely derive both cloud fraction and cloud optical thickness from the measured spectral reflectivity of a single pixel, as cloudy scenes with the same cloud top pressure but with different cloud fractions and cloud optical thicknesses may give rise to (almost) the same spectral reflectivity, both inside and outside the oxygen A band.

To demonstrate that this ambiguity in cloud fraction and cloud optical thickness does, in general, not lead to significant errors in the derived cloud top pressure, we performed multiple scattering calculations inside and outside the oxygen A band with a doubling-adding radiative transfer model [*De Haan et al.*, 1987; *Stammes*, 1994]. In these calculations, a midlatitude summer atmosphere was assumed and a nadir viewing direction. Molecular scattering was taken into account, as well as reflection by a Lambertian ground surface (with A_s=0.05 and 0.3). Cloud layers with a geometrical thickness of 1 km and different optical thicknesses, b_c, were inserted at various heights in the atmosphere. For the cloud particles we assumed a Henyey-Greenstein phase function with an asymmetry parameter of 0.85 and a single scattering albedo of 1. To simulate the reflectivity of a partly cloudy scene, the reflectivities of a cloud free and fully cloudy atmosphere were added, weighted with the area of the cloud-free and cloudy parts of the pixel. The reflectivities measured by GOME between 760 and 766 nm consist of contributions of many different oxygen absorption lines and are dominated by the wings of the lines because the central parts of the lines are completely saturated. We therefore performed calculations for four oxygen absorption optical thicknesses, b_{o_2}, which span a relevant range of oxygen (total column) optical thickness values between 760 and 766 nm: namely, for b_{o_2}=1.62, 0.35, 0.026, and 0. These values are the exponentially averaged absorption optical thicknesses in the 760–761 nm and 765–766 nm windows, the minimum absorption optical thickness in the wavelength interval 760–766 nm, and the absorption optical thickness outside the band, respectively. We did not convolute the calculated reflectivities with the GOME slit function, but this does not influence our conclusions based on the results of these calculations.

Calculations were made for (partly) cloudy cases for which we varied b_c between 0 and 100, c between 0 and 1, and P_c between 280 and 900 hPa. For each P_c value we considered cases with different values of b_c and c but with the same nadir reflectivity at the top of the atmosphere in the continuum, R_{con}. For these cases, referred to as (b_c,c) equivalent cases, we investigated the variation in the reflectivity at absorbing wavelengths. R_{con} was varied from 0.2 to 0.8, or a smaller range if these values of R_{con} could not be obtained for the given A_s and θ_0 values. As an example, Figures 3a–3d show nadir reflectivities inside the oxygen A band as functions of cloud top pressure, for R_{con}=0.5, A_s=0.05 and 0.30, and θ_0=30° and 75°. In Figures 3a–3d, different pairs of curves pertain to different oxygen absorption optical thicknesses. Within a pair the solid curve pertains to the cloudy case with maximum cloud fraction and minimum cloud optical thickness yielding R_{con}=0.5, and the dashed curve pertains to the cloudy case with minimum cloud fraction and maximum cloud optical thickness yielding R_{con}=0.5, i.e., the most extreme (b_c,c) equivalent cases. For example, in Figure 3a the solid curves pertain to c=1 and b_c=12, and the dashed curves pertain to c=0.48 and b_c=100. We conclude that for most cloud top pressures the variation in the reflectivity inside the O_2 A band due to variation in b_c and c is small if the reflectivity outside the O_2 A band is the same. In Figure 3 considerable variation in the reflectivity does occur only if A_s=0.3, θ_0=75° and b_{o_2}=0.35 (moderate absorption optical thickness). These results imply that for most cases, knowledge of the individual values of b_c and c is not needed in order to retrieve cloud top pressure from such reflectivity measurements, as long as the combination (b_c,c) yields the measured value in the continuum. Consequently, for surfaces with a low albedo the correct cloud top pressure can be retrieved if b_c (or A_c) is chosen a priori. Obviously, the derived cloud fraction is strongly coupled to the choice of A_c and must therefore be regarded as an effective cloud fraction. For surfaces with high albedo, however, our calculations show that errors in the derived cloud top pressure may occur by using the effective cloud fraction concept, particularly when R_{con} is only slightly higher than A_s. This is discussed further in section 3.6.

For various reasons, we have chosen a (high) cloud albedo of 0.8. First, from statistics of GOME measurements it appears that reflectivities of cloudy scenes

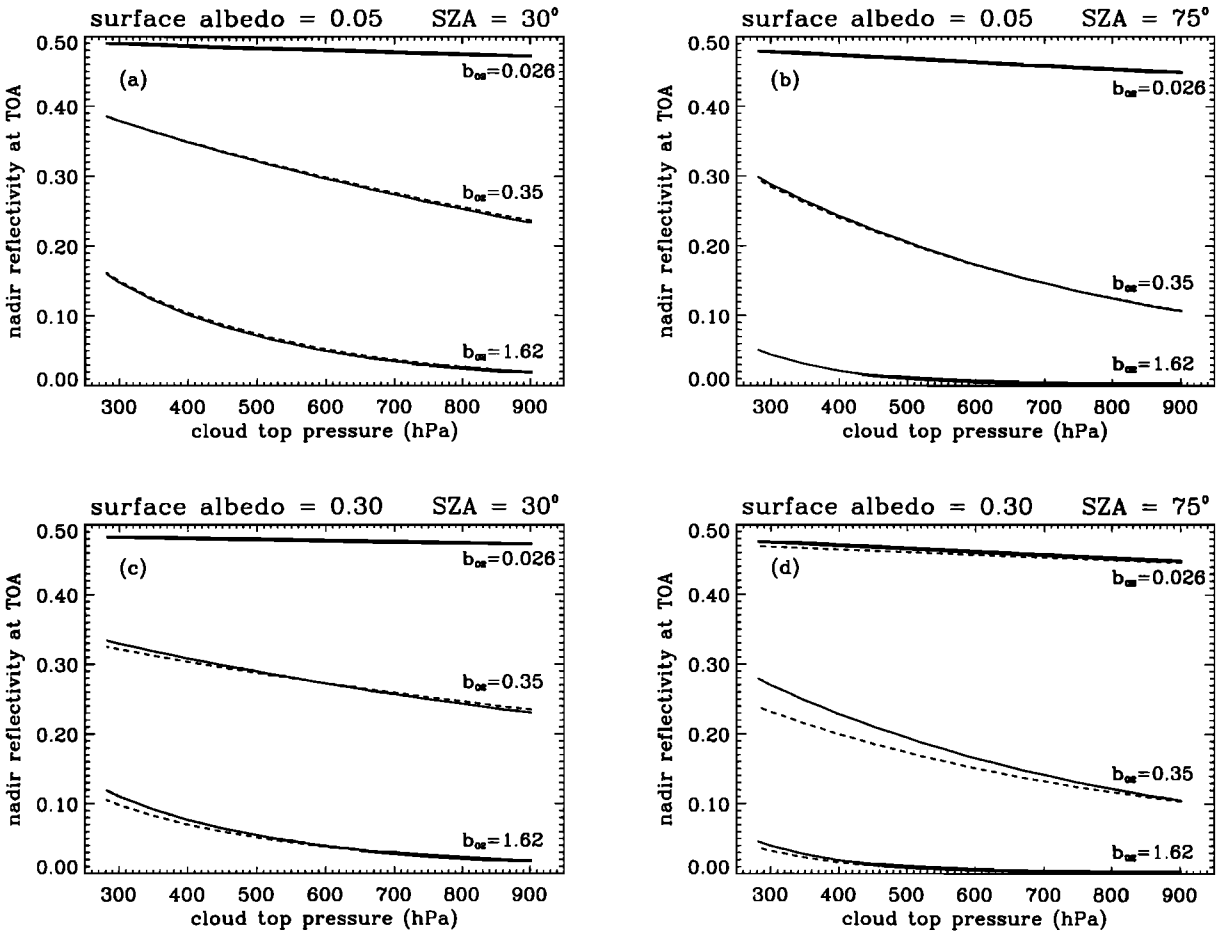

Figure 3. Nadir reflectivities in the O_2 A band for cloudy scenes with different cloud fractions and cloud optical thicknesses but with the same nadir reflectivity at the top of the atmosphere in the continuum (=0.5), as functions of cloud top pressure. Solid curves indicate maximum cloud fraction, minimum cloud optical thickness; dashed curves indicate minimum cloud fraction, maximum cloud optical thickness. Different pairs of curves pertain to different oxygen absorption optical thicknesses, namely, b_{o_2}=0.026, 0.35, and 1.62. Results are shown for different values of the surface albedo A_s and solar zenith angle θ_0, namely, $A_s = 0.05$, $\theta_0 = 30°$ (a); $A_s = 0.05$, $\theta_0 = 75°$ (b); $A_s = 0.30$, $\theta_0 = 30°$ (c); $A_s = 0.30$, $\theta_0 = 75°$ (d).

rarely exceed 0.8 at 758 nm but may quite often be larger than 0.6. Thus the smaller the value of A_c is chosen, the more often it will not be possible to approach the measured reflectivity with the simulations, as we restrict the effective cloud fractions to values between 0 and 1. By choosing a rather extreme value for the cloud albedo of 0.8 the effective cloud fraction is able to span a large range of cloudy situations which occur in reality. Second, in our bireflector model we assume that absorption below the cloud may be neglected. This approximation clearly breaks down for an optically thin cloud above a bright surface. Therefore a high cloud albedo has been assumed, so that the model assumptions are internally consistent. Third, in the current GOME ozone column density retrieval algorithm, absorption below the cloud is neglected as well. *Koelemeijer and Stammes* [1999b] show that the choice A_c=0.8 is optimal for cloud correction of ozone column density retrievals from GOME ultraviolet measurements. If a lower value for A_c is used, the correction which is applied to account for ozone below the cloud is too large.

3. Sensitivity Analysis

To investigate the sensitivity of the FRESCO effective cloud fractions and cloud top pressures to measurement errors and retrieval assumptions, a sensitivity study has been performed. Eight sensitivity experiments were carried out, to be described below, using real data from two GOME orbits; one orbit over Europe, Africa, and the Atlantic Ocean (ERS-2 orbit 1222) and one orbit over the Atlantic Ocean and South America (ERS-2 orbit 1223). The data were acquired on July 15, 1995. Approximately 75% of the pixels concerns sea and 25% concerns land. The GOME pixel size was 40 × 80 km^2. For these orbits the mean FRESCO effec-

Table 1. Results of Sensitivity Analysis of FRESCO

Experiment	Effective Cloud Fraction			Cloud Top Pressure, hPa			Remarks
	δ_c	σ_c	π_c	δ_{P_c}	σ_{P_c}	π_{P_c}	
$\lambda \pm 0.04$ nm	0.00	0.00	0.00	6	5	15	global
Radiometric errors	0.01	0.01	0.02	13	4	19	global
Tropical profile	0.00	0.00	0.00	1	1	2	global
$P_s \pm 20$ hPa	0.00	0.00	0.00	8	3	14	global
	0.00	0.00	0.00	7	2	11	sea
	0.00	0.00	0.00	11	4	20	land
$A_s \pm 0.02$	0.02	0.01	0.02	15	16	50	sea
	0.01	0.00	0.02	5	4	13	sea and $c > 0.3$
$A_s \pm 0.05$	0.05	0.03	0.09	53	79	191	land
	0.04	0.02	0.07	15	14	45	land and $c > 0.3$
$A_c = 0.6$	0.10	0.07	0.24	2	1	3	sea
	0.14	0.13	0.34	22	24	70	land
	0.21	0.13	0.39	16	14	42	land and $c > 0.3$
$R_c = R_c(\theta, \theta_0, \phi - \phi_0)$	0.04	0.06	0.16	1	1	3	sea
	0.02	0.04	0.05	5	9	18	land
	0.04	0.06	0.06	3	8	13	land and $c > 0.3$
Error-weighted fitting	0.00	0.00	0.01	26	26	81	global

tive cloud fraction is 0.33, and the mean FRESCO cloud top pressure is 691 hPa. We used real GOME measurements for this sensitivity study in order to have a realistic coverage of possible conditions. The orbits were selected such that the proportion of GOME pixels concerning land and sea is close to the global proportion of land and sea area. Furthermore, in the selected orbits, various land surface types are present, including desert. The orbits were selected arbitrarily in all other respects. We only considered pixels for which $\theta_0 \leq 80°$. Furthermore, for the cloud top pressure results, only those P_c values were considered for which c was larger than 0.1 because the error in the retrieved P_c becomes very large if the effective cloud fraction approaches zero.

In the sensitivity analysis we changed a certain parameter and considered the absolute differences in the retrieved effective cloud fractions or cloud top pressures between the perturbed case, in which the parameter is set to its changed value, and the reference case, in which the parameter has its usual value, as specified in section 2.2.2. The results of the sensitivity analysis are described in terms of the mean δ, the standard deviation σ, and the 95th percentile π of the absolute difference in the retrieved effective cloud fractions and cloud top pressures. These quantities have a suffix c if they correspond to an effective cloud fraction change and a suffix P_c if they correspond to a cloud top pressure change. The results of the sensitivity analysis have been summarized in Table 1. The various experiments mentioned in Table 1 will be discussed in sections 3.1–3.8. Absolute values have been considered because otherwise the mean differences would almost vanish if a parameter is changed in both positive and negative direction with respect to the reference value. When relevant, the sign of the change will be mentioned in the text. For some experiments the results of the sensitivity analysis depend on surface type (land or sea) or on the effective cloud fraction (assuming A_c=0.8), which, when appropriate, is indicated in the remarks column of Table 1.

3.1. Wavelength Calibration

The accuracy of the wavelength calibration of the GOME reflectivity at wavelengths of the O_2 A band is estimated to be ± 0.04 nm. Therefore we have studied the effect on the retrieved effective cloud fraction and cloud top pressure of a shift in the wavelength grid of the reflectivity measurements with $\Delta\lambda = \pm 0.04$ nm. As shown in the first row of Table 1, the resulting change in the retrieved effective cloud fraction is negligible, and the absolute change in the retrieved cloud top pressure is smaller than 15 hPa for 95% of the considered pixels.

3.2. Radiometric Calibration

The accuracy of the GOME reflectivities in the continuum at wavelengths around the O_2 A band is esti-

mated to be 2–3% [*Koelemeijer et al.*, 1998]. However, inside strong absorption bands the reflectivities are expected to be less accurate than in the continuum. This is related to the sensitivity of the GOME instrument to the degree of polarization of light entering the instrument and the fact that the GOME polarization correction method is designed for continuum wavelengths. However, in strong atmospheric absorption bands like the O_2 A band the degree of polarization of scattered light is generally different from that outside the band [*Stam et al.*, 1999]. From ground-based high spectral resolution polarization measurements of the cloud-free zenith sky with the GOME bread-board model [*Aben et al.*, 1999], it appears that the difference in the degree of polarization inside and outside the O_2 A band can be as much as 0.15. Using this value and the preflight measured polarization sensitivity of GOME, we estimated the error in the reflectivity at the top of the atmosphere inside the O_2 A band to be 5% or smaller, except for large solar zenith angles.

To investigate the effect of the above radiometric errors, we introduced a relative error in the GOME reflectivity measurements of ±2% at wavelengths where no oxygen absorption takes place, of ±5% for the wavelength at which the absorption is strongest, and a proportional error at wavelengths with intermediate absorption. We found that the effects on c and P_c were π_c=0.02 and π_{P_c}=19 hPa. These values are almost independent of surface albedo and effective cloud fraction.

3.3. Atmospheric Profile

In the simulations we used a midlatitude summer atmosphere. To investigate the influence of this choice on the FRESCO results, we replaced the midlatitude summer profile by a tropical profile [*Anderson et al.*, 1986]. In spite of the considerable difference between these atmospheric profiles, π_c and π_{P_c} are negligible compared to other uncertainties, which is in agreement with results of *Bréon and Bouffiès* [1996].

3.4. Surface Pressure

To investigate the influence of variations in the surface pressure, we varied P_s with ΔP_s=±20 hPa. It appears that the derived effective cloud fraction is insensitive to P_s; the derived global cloud top pressure has δ_{P_c}=8 hPa. The effect on the derived cloud top pressure is largest over areas with a high surface albedo and a small effective cloud fraction (see Table 1).

3.5. Surface Albedo

The surface albedo of sea is chosen to be 0.02. For land it is deduced from the surface albedo database described in section 2. The spatial resolution of the surface albedo database, 2.5° × 2.5°, is rather coarse. This was done to ensure that each grid box contains many GOME observations and thus to reduce the chance of cloud contamination in the database. However, the surface albedo of land may vary considerably within such a grid box. Therefore we varied the assumed surface albedo by ΔA_s=±0.05 for land. The surface albedo of sea is varied by ΔA_s=±0.02. The results are shown in Table 1.

The resulting change in effective cloud fraction agrees well with the change expected from the following simple consideration. For wavelengths in the continuum we

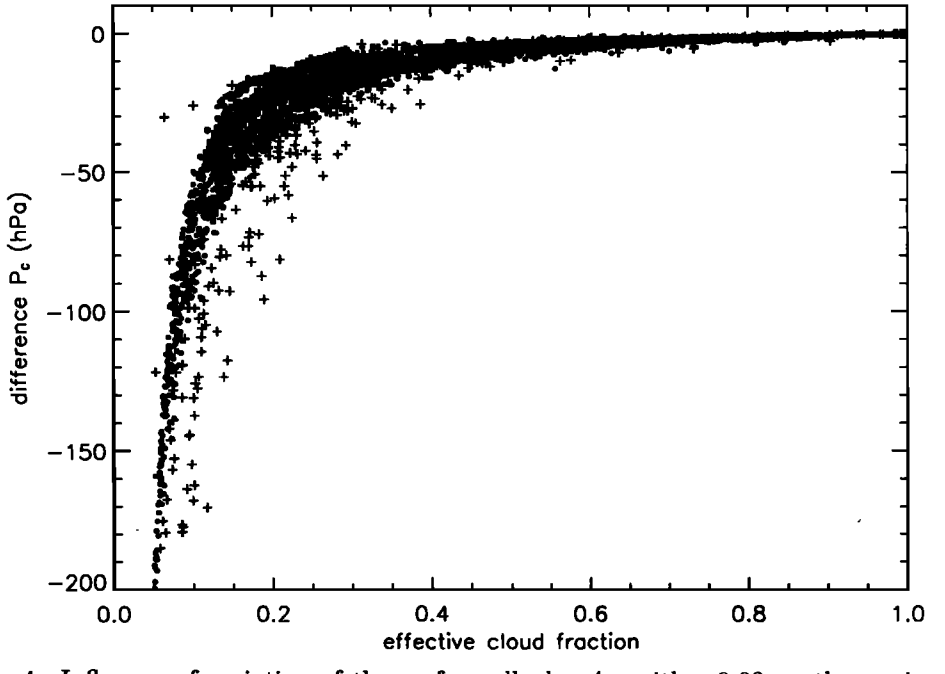

Figure 4. Influence of variation of the surface albedo, A_s, with +0.02 on the retrieved cloud top pressure, as a function of the effective cloud fraction. Dots indicate clouds over sea, crosses indicate clouds over land.

may set $\bar{T} = 1$ in (9). Using $R_{\text{sim}}(\lambda) \approx R_{\text{meas}}(\lambda)$, we then find

$$c = \frac{R_{\text{meas}} - A_s}{A_c - A_s}. \tag{10}$$

Differentiation to A_s gives the change in the retrieved effective cloud fraction, Δc, due to a small change in the assumed surface albedo, ΔA_s:

$$\Delta c = -\frac{1-c}{A_c - A_s}\Delta A_s. \tag{11}$$

Thus the effective cloud fraction is reduced if A_s is increased, as $A_c - A_s > 0$. Equation (11) also shows that the retrieved effective cloud fraction is particularly sensitive to changes in the assumed surface albedo if the surface albedo is high.

The derived cloud top pressure is sensitive to errors in the surface albedo when the effective cloud fraction is small and, to a lesser extent, when the surface albedo is high. This is apparent from Figure 4, which shows the difference in the retrieved cloud top pressure (perturbed case minus reference case) as a function of effective cloud fraction, for $\Delta A_s = 0.02$, both for land and sea. Clearly, if the effective cloud fraction is small, errors in the surface albedo lead to large relative errors in the effective cloud fraction and therefore to large absolute errors in the cloud top pressure. From Table 1 it can be observed that for sea, and if c is larger than 0.3, the derived cloud top pressure is rather insensitive to errors in the surface albedo (π_{P_c}=13 hPa for $\Delta A_s = 0.02$).

3.6. Cloud Albedo

To investigate the influence of the assumption A_c=0.8 on the retrieved effective cloud fraction and cloud top pressure, we compared it to the assumption A_c=0.6. Again, the results are shown in Table 1. The change in the retrieved effective cloud fraction follows from differentiation of (10) to A_c, which gives

$$\Delta c = -\frac{c}{A_c - A_s}\Delta A_c. \tag{12}$$

Thus the relative increase in c is proportional to a decrease in A_c, and the relative change is large if $A_c - A_s$ is small, i.e., over bright surfaces. We do not regard the change in c related to the chosen A_c as an error in the derived c, but rather, we interpret the derived c in the reference case as an effective cloud fraction, which is the cloud fraction obtained by assuming A_c=0.8. A similar assumption should be made in the subsequent use of this effective cloud fraction, e.g., for air mass factor calculations for ozone [*Koelemeijer and Stammes*, 1999b].

As is shown in Table 1, if the surface albedo is close to zero, such as for ocean, the cloud top pressure is insensitive to the chosen cloud albedo because of the following reasoning. If A_s=0, (9) reduces to

$$R_{\text{sim}} = cA_c\bar{T}(\lambda, P_c, \theta, \theta_0). \tag{13}$$

During the fitting process the product cA_c and the transmission $\bar{T}$ now behave in an uncoupled fashion. This means that different combinations of c and A_c which yield the same R_{sim} outside the O_2 A band also yield the same R_{sim} inside the band. Consequently, the P_c value needed to fit the measurements will not depend on A_c. In case the surface albedo is much larger than zero, we do find a dependence of P_c on A_c. This indicates that our bireflector model behaves similar in this respect to the more comprehensive doubling-adding model in which absorption inside and below the cloud was taken into account (see section 2.2.3). As shown in Table 1, for land surfaces and if $c > 0.3$, 95% of the data has a change in the retrieved cloud top pressure of 42 hPa or smaller when changing from A_c=0.8 to A_c=0.6.

3.7. Bidirectional Effect of Clouds

To investigate the influence of cloud bidirectional effects on the retrieved c and P_c, we replaced the cloud albedo A_c in our retrieval algorithm by a bidirectional reflectivity $R_c = R_c(b_c, \theta, \theta_0, \phi - \phi_0)$, where b_c is the cloud optical thickness and $\phi - \phi_0$ is the azimuth difference between the directions of the satellite and the Sun. To calculate the cloud bidirectional reflectivity, we assumed a two-parameter gamma cloud droplet size distribution with an effective radius of r_e=6 μm and an effective variance of v_e=1/9 (the C1 model of *Deirmendjian* [1969, p. 78]), for which the single scattering properties were calculated using Mie theory [*De Rooij and Van der Stap*, 1984]. The multiple scattering was calculated with the doubling-adding model. In the calculations we have chosen an optical thickness of b_c=33.9, so that the spherical albedo of the cloud equals 0.8.

The results are given in Table 1. We verified that the change in c is in agreement with (12) if ΔA_c is replaced by $(R_c - 0.8)$. We found that changes in the retrieved c and P_c are largest for large solar zenith angles because then R_c deviates most from A_c. Also, δ_{P_c} is small over sea surfaces and is relatively large over land surfaces with a small effective cloud fraction. In general, both δ_c and δ_{P_c} are smaller than those of the cloud albedo experiment described in section 3.6.

3.8. Fitting Method

To minimize the difference between $R_{\text{sim}}(\lambda)$ and $R_{\text{meas}}(\lambda)$, the reflectivities at the different wavelengths have been given the same weight, referred to as unweighted fitting. Another approach is to weight the reflectivities by the measurement error, referred to as weighted fitting. In this section we compare these two fitting methods. For the weighted fitting, the measurement errors are taken the same as specified in section 3.2. As shown in Table 1, the difference between the two fitting methods is negligible for effective cloud fractions. For the cloud top pressures, however, the influence is considerable. Using weighted fitting, the derived cloud top pressures are 26 hPa lower than using unweighted fitting, on average. To discuss the differ-

Table 2. Statistics of Residual Difference Between Simulated and Measured Reflectivity for the Three 1-nm-Wide Wavelength Windows

	758–759 nm		760–761 nm		765–766 nm	
Fitting Method	δ_ϵ	σ_ϵ	δ_ϵ	σ_ϵ	δ_ϵ	σ_ϵ
Unweighted	-0.0023	0.0021	-0.0026	0.0027	0.0030	0.0031
Weighted	-0.0043	0.0033	0.0004	0.0005	0.0049	0.0047

ences, we consider the residual errors $\epsilon = R_{\text{sim}} - R_{\text{meas}}$, averaged over the five wavelengths in each of the three windows. The average residual error, δ_ϵ (averaged over all pixels), and standard deviation of the residual error, σ_ϵ, are given in Table 2 for the three wavelength windows. The average residual errors are small but significantly different from zero. If our retrieval model would include all physical processes which occur in reality, it would be possible to make the average residual error arbitrary small, irrespective of the fitting method (assuming random measurement errors and averaging over sufficient pixels). Thus the fact that the average residual error does not vanish indicates shortcomings of the model. Apparently, these shortcomings typically give rise to retrieval errors in P_c due to the fitting method of 26 hPa.

4. Cloud Retrieval Method for ATSR-2 Data

In order to validate the FRESCO algorithm applied to GOME data, colocated measurements of the Along Track Scanning Radiometer-2 (ATSR-2) [*Mutlow et al.*, 1994] have been analyzed to yield an effective cloud fraction and cloud top pressure. The ATSR-2 has seven channels, at 0.55, 0.66, 0.87, 1.6, 3.7, 11, and 12 μm, and has a pixel size of 1×1 km^2 subsatellite. The shortwave radiance measurements of ATSR-2 are converted to reflectivity using solar irradiance measurements made by ATSR-2 (see equation (4)). The thermal infrared measurements are compared to on-board blackbodies (which have an emissivity of 1) and are expressed as (apparent) brightness temperatures in the ATSR-2 data product. Fourteen ATSR-2 images of 512×512 km^2 were analyzed, acquired over northwest Europe and the Atlantic Ocean on July 23, 1995. The data concern parts of ERS-2 orbits 1336 (mainly over land) and 1337 (mainly over sea). For these data the solar zenith angle was between 26° to 55°.

As a first step to derive cloud parameters, we developed a cloud detection algorithm to separate cloud-free and cloudy pixels in an ATSR-2 image. This algorithm employs four standard cloud detection tests to decide if a pixel is cloudy or clear, similar to the work of *Saunders and Kriebel* [1988]. In the cloud detection algorithm, reflectivity measurements made at 0.66 and 0.87 μm, denoted by $R_{0.66}$ and $R_{0.87}$, are used, as well as brightness temperature measurements made at 11 and 12 μm, denoted by T_{11} and T_{12}. If one of the tests determines the pixel as cloudy, it is designated as a cloudy pixel; only if all tests indicate that a pixel is cloud-free, it is designated as a clear pixel. The first test makes use of the fact that clouds are generally brighter than the surface. Therefore, if $R_{0.66}$ exceeds a specified threshold, the pixel is designated as cloudy. The second test makes use of the fact that clouds are generally colder than the surface. Therefore, if T_{11} is lower than a certain threshold, the pixel is designated as cloudy. The third test considers the spectral reflectivity of the pixel. Since clouds are generally whiter than the surface, a pixel is designated as cloudy if the ratio $R_{0.87}/R_{0.66}$ is close to unity. The fourth test is used to detect semitransparent clouds by considering the brightness temperature difference $T_{11} - T_{12}$, which is large for semi-transparent clouds, but small for cloud-free scenes and for optically thick clouds. The thresholds are determined from histogram analysis. The cloud-free pixels are used to obtain R_{land} and R_{sea}, which are the average reflectivities of the cloud-free land and sea pixels in an ATSR-2 image, respectively.

After cloud detection, an effective cloud fraction c is derived for each part of an ATSR-2 image which corresponds to a GOME pixel according to (compare (10))

$$c = \frac{R_{0.66} - R_{\text{clear}}}{R_{\text{cloud}} - R_{\text{clear}}}, \tag{14}$$

where R_{clear} and R_{cloud} are the reflectivities which would be measured if the whole GOME pixel were clear and fully covered by optically thick clouds, respectively. R_{clear} is calculated from

$$R_{\text{clear}} = f_{\text{land}} R_{\text{land}} + (1 - f_{\text{land}}) R_{\text{sea}}, \tag{15}$$

where f_{land} is the fraction of the ATSR-2 pixels inside the GOME pixel pertaining to land. A land/sea mask is supplied in the ATSR-2 data product. In FRESCO we use R_{cloud}=0.8 for wavelengths between 758 and 766 nm. To be consistent with this assumption in FRESCO, we use R_{cloud}=0.77 at 660 nm in our ATSR-2 algorithm. This value is lower than 0.8 because we take into account ozone absorption in the Chappuis band at 660 nm. Calculations with the doubling-adding method (see section 3.7) show that if R_{cloud}=0.8 at 760 nm, R_{cloud}=0.77±0.005 at 660 nm, for the solar zenith an-

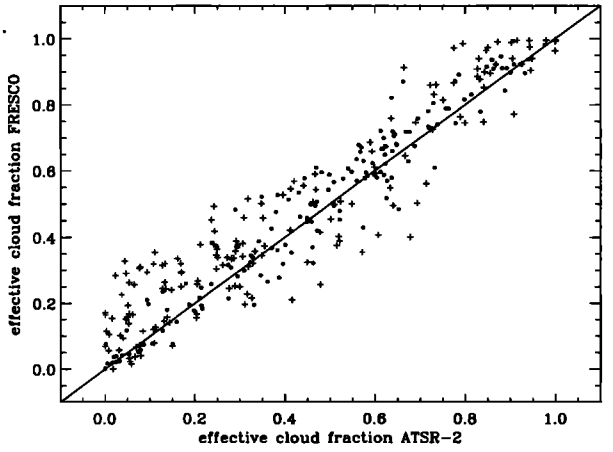

Figure 5. Correlation between FRESCO and ATSR-2 effective cloud fractions. The data were acquired on July 23, 1995, over northwest Europe, and are parts of ERS-2 orbits 1336 and 1337. Dots indicate clouds over sea, crosses indicate clouds over land.

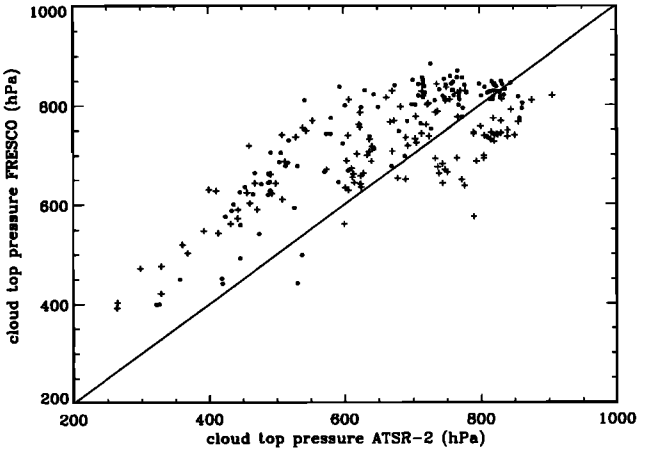

Figure 6. Same as Figure 5, but for cloud top pressures.

gle and cloud top pressures ranges which occur for the selected GOME and ATSR-2 data.

To derive cloud top pressure, 11-μm brightness temperature measurements of the cloudy ATSR-2 pixels were converted to pressures using temperature profiles from the analyzed fields of the European Center for Medium-range Weather Forecasts (ECMWF) model. The ATSR-2 brightness temperature is a good measure for the cloud top temperature only if (1) the emissivity of the cloud is close to unity and (2) the absorption and emission of the atmosphere above the cloud can be neglected. Because the atmosphere is almost transparent at 11 μm, we assumed that the second condition is satisfied. The first condition holds for clouds which have a small temperature difference $T_{11} - T_{12}$. Therefore only those cloudy ATSR-2 pixels in a GOME pixel were selected which fulfilled the emissivity criterion $T_{11} - T_{12} \leq 1$ K. The cloud top pressures of these ATSR-2 pixels have been averaged to obtain the ATSR-2 cloud top pressure pertaining to the GOME pixel, which is briefly referred to as the ATSR-2 cloud top pressure.

Often, only a fraction of all ATSR-2 pixels inside the GOME pixel fulfill the emissivity criterion, in which case, the ATSR-2-derived cloud top pressure may not be representative for the whole GOME pixel. Therefore, in our comparison of FRESCO- and ATSR-2-derived cloud top pressures, we only considered GOME pixels in which more than 15% of the ATSR-2 pixels fulfilled the emissivity criterion. In section 6 we will show that the threshold of 15% appears to be a reasonable value. Furthermore, in the comparison of FRESCO and ATSR-2 derived cloud top pressures, we only considered GOME pixels for which the FRESCO effective cloud fraction was larger than 0.1. Among the 322 pixels, 236 pixels fulfilled these selection criteria.

5. Comparison of FRESCO and ATSR-2 Cloud Parameters

The correlation between the effective cloud fractions from FRESCO and ATSR-2 is shown in Figure 5, and the correlation between the cloud top pressures from FRESCO and ATSR-2 is shown in Figure 6. The dots correspond to clouds above sea and the crosses correspond to clouds above land. Table 3 lists the number of pixels used for the comparison, N; the average difference (FRESCO − ATSR-2), δ; the standard deviation, σ; the 95th percentile, π; and the linear correlation coefficient, r, of the FRESCO and ATSR-2 effective cloud fractions and cloud top pressures. These quantities have a subscript c if they pertain to effective cloud fraction and a subscript P_c if they pertain to cloud top pressure. The results are given for all pixels and separately for land and sea.

For the effective cloud fraction a good correlation is found, although FRESCO effective cloud fractions are slightly higher than those of ATSR-2. The average dif-

Table 3. Statistics of Difference Between FRESCO and ATSR-2 Cloud Parameters

Effective Cloud Fraction					Cloud Top Pressure, hPa					
N_c	δ_c	σ_c	π_c	r_c	N_{P_c}	δ_{P_c}	σ_{P_c}	π_{P_c}	r_{P_c}	Remarks
322	0.04	0.09	0.20	0.95	236	65	92	207	0.78	all pixels
152	0.02	0.07	0.14	0.97	117	84	76	199	0.85	sea pixels
170	0.05	0.11	0.23	0.94	119	46	102	216	0.74	land pixels

ference between FRESCO and ATSR-2 effective cloud fractions is 0.04 and the standard deviation is 0.09. The correlation is better for clouds over sea than over land due to the larger uncertainty in the surface albedo of land. The surface albedo of land, particularly vegetated land, is generally higher at wavelengths used by FRESCO (~760 nm) than at the wavelengths used by ATSR-2 (660 nm), whereas the sea surface albedo is low at both wavelengths. Therefore accurate determination of the effective cloud fraction is more difficult for clouds over land than for clouds over sea in FRESCO.

For cloud top pressures the correlation between FRESCO and ATSR-2 is weaker than for effective cloud fractions and shows more scatter. The average difference in cloud top pressure is 65 hPa and the standard deviation is 92 hPa. For clouds over sea the average difference is larger than for clouds over land, but the standard deviation is smaller. From Figure 6 it is clear that the FRESCO cloud top pressures are generally higher than the ATSR-2 cloud top pressures. For a number of cases, however, the situation is opposite, which we will consider first. From visual inspection of the ATSR-2 images it appears that these cases correspond almost entirely to scattered small-scale cumulus clouds. It is possible that the ATSR-2 pixels are not completely filled by these clouds but may be partly clear. These pixels are indicated as cloudy by our algorithm and also fulfill the emissivity criterion, which only rejects optically thin clouds but retains pixels partly covered by optically thick clouds and partly by cloud-free area. For partly cloudy pixels the P_c values derived from ATSR-2 will be a mixture of the true P_c and P_s. This is reinforced by the fact that the surface has a dominant contribution to the measured radiance by the ATSR-2 because the surface is warmer than the cloud top and the emitted radiation is strongly temperature-dependent according to the Planck function. Therefore it is likely that for these cases the ATSR-2-derived cloud top pressures have a bias toward higher pressures, thereby masking the systematic error in the FRESCO cloud top pressures. In the data set considered, these small-scale cumulus clouds are most often present over land. If these cases would be excluded, the statistical results for clouds over land would become similar to those over sea. In section 6 we will discuss possible causes for the systematic difference between FRESCO and ATSR-2 cloud top pressures.

6. Discussion

Considering the results of the sensitivity analysis in section 3, only errors in the assumed A_s or A_c, or the fitting method (error weighted or not), could give rise to systematic cloud top pressure errors of the magnitude given in Table 3. If the difference is due to errors in A_s or A_c, the difference should be dependent on surface type (land/sea) and should decrease with increasing effective cloud fraction. However, the difference in the retrieved cloud top pressures is not smaller over sea than over land, nor does it decrease with increasing effective cloud fraction. Therefore it is unlikely that the systematic difference in the derived P_c is due to errors in A_s or A_c. Alternatively, using the error-weighted fitting method, the systematic difference in the derived P_c decreases from 65 to 49 hPa; the standard deviation decreases only slightly, from 92 to 89 hPa, and the correlation coefficient improves slightly, from 0.78 to 0.80. Although the systematic error decreases, it does not vanish with the error-weighted fitting method. One could argue that it would be better to use the error-weighted fitting method, or use A_c=0.6 (a less extreme value for the cloud albedo) instead of A_c=0.8. For clouds over land, both changes are of similar order of magnitude and have opposite effects on the derived cloud top pressures. Therefore, if both changes are made simultaneously to FRESCO, the derived cloud top pressure values for clouds over land would only be slightly different from the values presented here. For clouds over sea the derived pressures in FRESCO would be lower by ~25 hPa on average.

A number of possible causes, other than those discussed in section 3, for the differences between ATSR-2- and FRESCO-derived cloud top pressures were considered, the conclusions of which are summarized here. A general concern is the quality of the temperature profiles used to convert the ATSR-2 brightness temperatures to pressures. The ECMWF results hold for July 23, 1995, 1200 UT. This is close to the acquisition time of the orbit 1337 data (within 15 min), but the time difference with the orbit 1336 data is almost 2 hours. Furthermore, the temperature profiles do not capture small-scale variations, in particular, inversions which may occur near cloud tops over a small altitude range. If inversions are present near the cloud top, the ATSR-2-derived cloud top pressures may have a bias toward

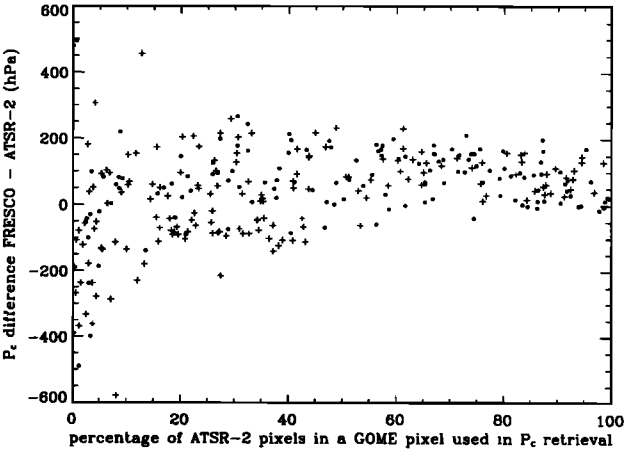

Figure 7. Difference between FRESCO- and ATSR-2-derived cloud top pressures as a function of the percentage of the ATSR-2 pixels in a GOME pixel that was used to retrieve the cloud top pressure from ATSR-2 measurements.

lower pressures and could explain part of the systematic difference.

Another concern is that the FRESCO cloud top pressures always pertain to the whole GOME pixel, whereas the ATSR-2 cloud top pressures pertain to a part of this pixel, as only cloudy ATSR-2 pixels were selected which fulfilled the emissivity criterion. An estimation of the impact of this effect can be obtained from Figure 7, which shows the difference between FRESCO and ATSR-2 derived cloud top pressures as a function of the percentage of ATSR-2 pixels inside the GOME pixel which fulfill the emissivity criterion. Clearly, if only a small percentage of ATSR-2 pixels fulfill the emissivity criterion (particularly when the percentage drops below 15%), the ATSR-2 cloud top pressure deviates strongly from the FRESCO cloud top pressure, indicating that it is no longer representative for the whole GOME pixel. It appears that the scatter between ATSR-2- and FRESCO-derived cloud top pressures decreases as the number of ATSR-2 pixels from which cloud top pressure is retrieved increases, and this may explain the random difference to some extent. The systematic difference remains, however, even for cases where almost all ATSR-2 pixels inside the GOME pixel can be used.

Interestingly, a correlation was found between the cloud top pressure difference FRESCO − ATSR-2 and the average cloud top reflectivity of the cloudy pixels as derived from the ATSR-2 measurements at 0.66 μm. Figure 8 shows this correlation for orbit 1337. Often, for clouds with a high reflectivity, corresponding to optically thick clouds, the difference in the retrieved cloud top pressures is large, whereas for optically thinner clouds, the difference is smaller. The general systematic difference between FRESCO- and ATSR-2-derived cloud fractions might be explained as follows: At thermal infrared wavelengths the transmission of clouds with an emissivity close to unity is smaller than their transmission at near-infrared wavelengths. Therefore, at thermal-infrared wavelengths the radiance detected by the satellite comes from higher parts of the cloud than at near-infrared wavelengths. However, the absorption by oxygen associated with photon paths inside and below the cloud is not taken into account in our simple bireflector model. Consequently, we may expect that the cloud top pressures retrieved by FRESCO will be biased toward higher values. To estimate the influence of neglecting absorption inside a cloud, we compared reflectivities obtained with the doubling-adding model presented in section 2.2.3 with reflectivities obtained with the bireflector model. We found that the error in the retrieved cloud top pressure due to neglecting absorption inside the cloud is of the order of 50–100 hPa for the conditions pertaining to the observations. The neglection of absorption within the cloud may lead to less accurate results for optically thick clouds than for optically thin clouds for the cloud systems considered. Often, the optical thickness of clouds is proportional

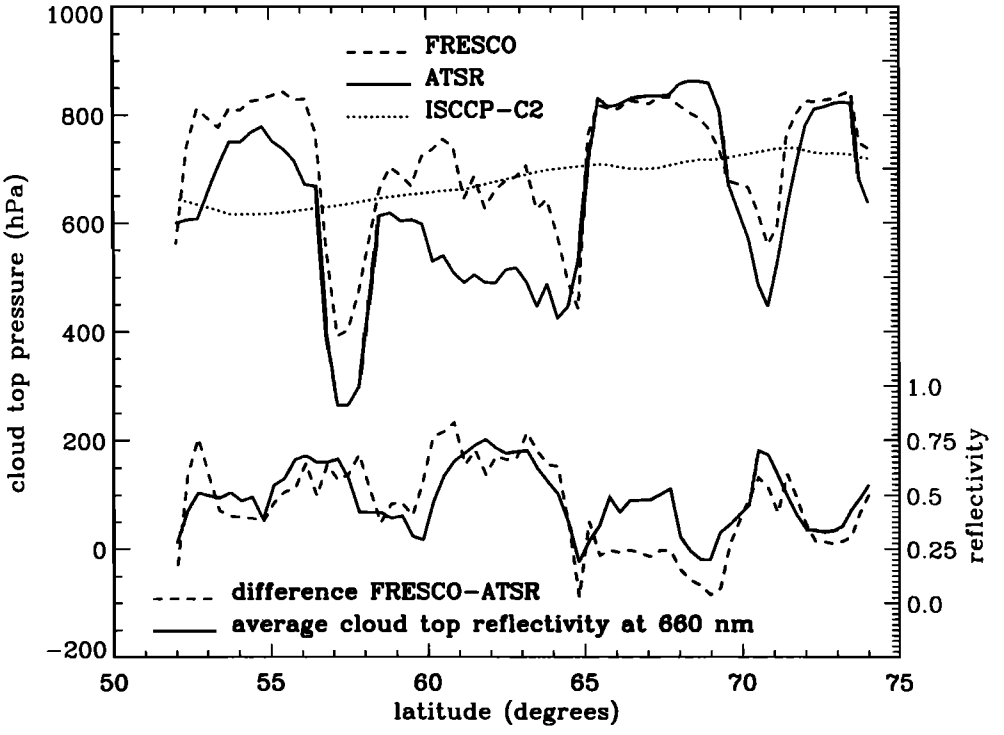

Figure 8. Cloud top pressures of FRESCO and ATSR-2, as well as their difference, in hPa. For comparison, the monthly average cloud top pressures from the ISCCP climatology are shown as well. The vertical axis on the right hand side pertains to the average cloud top reflectivity. The FRESCO and ATSR-2 data are from ERS-2 orbit 1337.

to their geometrical thickness [*Feigelson*, 1984]. The bireflector model gives most accurate results for cases for which the path inside and below the cloud is small, i.e., for optically and geometrically thin clouds above a dark surface. This may explain the smaller cloud top pressure differences for the optically thinner clouds. We conclude that it is likely that neglecting absorption inside and below the cloud is the main reason for the observed bias between FRESCO- and ATSR-2-retrieved cloud top pressures.

Despite the above described limitations, we expect that the use of the FRESCO effective cloud fractions and cloud top pressures is a significant improvement for cloud correction in column density retrievals of ozone and other trace gases. For comparison, we note that the average error in the effective cloud fractions derived by ICFA, which are presently used in the operational GOME data processor, is 0.18 and has a standard deviation of 0.23, as compared to effective cloud fractions derived from ATSR-2 data [*Koelemeijer and Stammes*, 1999a]. Furthermore, the errors in the assumed cloud top pressures, which are presently taken from the ISCCP climatology in the GOME data processor, can often be as large as 200 hPa, as can be seen in Figure 8. Such errors in effective cloud fractions and cloud top pressures can lead to considerable errors in ozone column retrieval, as has been quantified by *Koelemeijer and Stammes* [1999b].

7. Conclusions and Outlook

A simple bireflector model was used in our fast algorithm, called FRESCO, to derive an effective cloud fraction and cloud top pressure simultaneously from spectral measurements by GOME in and around the O_2 A band. The effective cloud fraction concept works well for dark surfaces, such as ocean, but may give rise to nonnegligible cloud top pressure retrieval errors above bright surfaces, even when the surface albedo is accurately known.

An analysis was performed to investigate the sensitivity of the retrieved effective cloud fraction and cloud top pressure to a priori assumptions and measurement errors. We found that the pressures derived with the O_2 A band method are insensitive to the assumed temperature profile. Besides errors due to neglecting absorption inside the cloud, the retrieved effective cloud fractions and cloud top pressures are primarily sensitive to errors in the assumed surface and cloud albedo. The retrieved cloud top pressure is particularly sensitive to errors in the surface albedo and cloud albedo for scenes above land with a small effective cloud fraction.

A good correlation was found between FRESCO effective cloud fractions and effective cloud fractions derived from colocated ATSR-2 measurements. The average difference between FRESCO and ATSR-2 effective cloud fractions is 0.04 and the standard deviation is 0.09. A reasonable correlation was found between FRESCO and ATSR-2 cloud top pressures. The average difference in cloud top pressure is 65 hPa and the standard deviation is 92 hPa. The systematic difference is most likely due to neglecting absorption inside the cloud in the FRESCO algorithm.

We would like to emphasize that the FRESCO and ATSR-2 algorithms to derive cloud top pressure are completely different, as FRESCO employs the oxygen A band, which is in the shortwave part of the Earth's spectrum, whereas ATSR-2 uses the thermal infrared part of the Earth's spectrum. The advantage of the O_2 A band method as compared to the brightness temperature method is that the first method is directly sensitive to pressure, whereas the latter method depends critically on the quality of the temperature profile used to convert brightness temperatures to pressures. A disadvantage of FRESCO is that treatment of oxygen absorption inside the cloud is necessary to obtain cloud top pressure retrieval errors below the 100 hPa error level.

In the future, we plan to improve the FRESCO effective cloud fraction and cloud top pressure retrieval by increasing the spatial resolution of the land surface albedo database and taking into account the temporal variation of the surface albedo. Furthermore, we plan to study the residual differences between our FRESCO model and the GOME measurements in more detail, as they may reveal information on photon paths in the real atmosphere. Nevertheless, the use of FRESCO cloud top pressures in its present form would be a significant improvement in the cloud correction of GOME ozone vertical column density retrievals, as compared to using a climatological value for the cloud top pressure. The FRESCO effective cloud fractions and cloud top pressures are presently used for near-real-time ozone column density retrieval at KNMI, in the framework of the GOME Ozone Fast Delivery and Value-Added Products project [*Piters et al.*, 1999; see also http://www.knmi.nl/gome_fd]. We expect that the FRESCO method is useful for the successors of GOME as well, such as Sciamachy, planned for launch on board Envisat in 2001, and the GOME-2 instruments on board the Metop series, the first of which is planned for launch in 2003. Another possible application of the FRESCO effective cloud fractions and cloud top pressures could be their use to determine the tropospheric column density of ozone, as demonstrated by *Ziemke et al.* [1998].

Acknowledgments. The European Space Agency (ESA) is acknowledged for kindly providing the GOME and ATSR-2 data through the Deutsches Zentrum für Luft- und Raumfahrt (DLR) and the European Space Research Institute (ESRIN). We would like to thank B. van den Hurk (KNMI) for his help with the ECMWF data. We are grateful to two anonymous reviewers for their comments on a draft version of this paper. Financial support for this work by the Space Research Organization of the Netherlands (SRON), the Netherlands Agency for Aerospace Programs (NIVR), and the Netherlands Remote Sensing Board (BCRS) is acknowledged.

References

Aben, I., F. Helderman, D. M. Stam, and P. Stammes, Spectral fine-structure in the polarisation of skylight, *Geophys. Res. Lett., 26,* 591-594, 1999.

Anderson, G. P., S. A. Clough, F. X. Kneizys, J. H. Chetwynd, and E. P. Shettle, AFGL atmospheric constituent profiles, *Tech. Rep. AFGL-TR-86-0110,* Air Force Geophys. Lab., Hanscom AFB, Mass., 1986.

Bréon, F.-M., and S. Bouffiès, Land surface pressure estimate from measurements in the O_2 A-band, *J. Appl. Meteorol., 35,* 67-77, 1996.

Burrows, J. P., et al., The Global Ozone Monitoring Experiment (GOME): Mission concept and first scientific results, *J. Atmos. Sci., 56,* 151-175, 1999.

Caspar, C., and K. Chance, GOME wavelength calibration using solar and atmospheric spectra, in *Proceedings of the third ERS symposium, Florence, Italy, 17-21 March 1997, Eur. Space Agency Spec. Publ. ESA SP-414,* pp. 609-614, 1997.

Chapman, R. M., Cloud distributions and altitude profiles from a satellite, *Planet. Space Sci., 9,* 71, 1962.

De Haan, J. F., P. B. Bosma, and J. W. Hovenier, The adding method for multiple scattering calculations of polarized light, *Astron. Astrophys., 183,* 371-391, 1987.

Deirmendjian, D., *Electromagnetic Scattering on Spherical Polydispersions,* 290 pp., Elsevier Sci., New York, 1969.

De Rooij, W. A., and C. C. A. H. Van der Stap, Expansion of Mie scattering matrices in generalized spherical functions, *Astron. Astrophys., 131,* 237-248, 1984.

Deutsches Zentrum für Luft- und Raumfahrt (DLR), GOME level 1 to 2 algorithms description, *Tech. Rep. ER-TN-DLR-GO-0025,* 32 pp., Oberpfaffenhofen, Germany, 1994.

European Space Agency (ESA), A study of cloud detection–Final report, *Tech. Rep. ESA Contract 10997/94/ NL/CN,* Noordwijk, Netherlands, 1996.

Feigelson, E. M., *Radiation in a Cloudy Atmosphere,* 293 pp., D. Reidel, Norwell, Mass., 1984.

Fischer, J., and H. Grassl, Detection of cloud-top height from backscattered radiances within the oxygen A band, part 1, Theoretical study, *J. Appl. Meteorol., 30,* 1245-1259, 1991.

Fischer, J., W. Cordes, A. Schmitz-Peiffer, W. Renger, and P. Mörl, Detection of cloud-top height from backscattered radiances within the oxygen A band, Part 2, Measurements, *J. Appl. Meteorol., 30,* 1260-1267, 1991.

Gamache, R. R., A. Goldman, and L. S. Rothman, Improved spectral parameters for the three most abundant isotopomers of the oxygen molecule, *J. Quant. Spectrosc. Radiat. Transfer, 59,* 495-509, 1998.

Joiner, J., and P. K. Bhartia, The determination of cloud pressures from rotational Raman scattering in satellite backscatter ultraviolet measurements, *J. Geophys. Res., 100,* 23,019-23,026, 1995.

Knibbe, W. J. J., J. F. de Haan, J. W. Hovenier, D. M. Stam, R. B. A. Koelemeijer, and P. Stammes, Deriving terrestrial cloud top pressure from photopolarimetry of reflected light, *J. Quantit. Spectrosc. Radiat. Transfer, 64,* 173-199, 2000.

Koelemeijer, R. B. A. and P. Stammes, Validation of Global Ozone Monitoring Experiment cloud fractions relevant for accurate ozone column retrieval, *J. Geophys. Res., 104,* 18,801-18,814, 1999a.

Koelemeijer, R. B. A. and P. Stammes, Effects of clouds on ozone column retrieval from GOME UV measurements, *J. Geophys. Res., 104,* 8281-8294, 1999b.

Koelemeijer, R. B. A., P. Stammes, and P. D. Watts, Comparison of visible calibrations of GOME and ATSR-2, *Remote Sens. Environ., 63,* 279-288, 1998.

Kollewe, M., W. Cordes, and J. Fischer, Measurement and interpretation of the sunlight backscattered from clouds within the oxygen-A absorption band, in *Proceedings of the Central Symposium of the International Space Year, Munich, Germany, 30 March - 4 April 1992, Eur. Space Agency Spec. Publ. ESA SP-341,* pp. 311-315, 1992.

Kuze, A., and K. V. Chance, Analysis of cloud top height and cloud coverage from satellites using the O_2 A and B bands, *J. Geophys. Res., 99,* 14,481-14,491, 1994.

Mutlow, C. T., A. M. Zàvody, I. J. Barton, and D. T. Llewellyn-Jones, Sea surface temperature measurements by the along-track scanning radiometer on the ERS-1 satellite: Early results, *J. Geophys. Res., 99,* 22,575-22,588, 1994.

O'Brien, D. M., and R. M. Mitchell, Error estimates for retrieval of cloud-top pressure using absorption in the A band of oxygen, *J. Appl. Meteorol., 31,* 1179-1192, 1992.

Piters, A. J. M., P. J. M. Valks, R. B. A. Koelemeijer, and D. M. Stam, GOME ozone fast delivery and value-added products algorithm specification document, *Tech. Rep. GOFAP-KNMI-ASD-01,* 23 pp., R. Neth. Meteorol. Inst., De Bilt, Netherlands, 1999.

Prata, A. J., and P. J. Turner, Cloud-top height determination using ATSR data, *Remote Sens. Environ., 59,* 1-13, 1997.

Press, W. H., B. P. Flannery, S. A. Teukolsky, and W. T. Vetterling, *Numerical Recipes,* 818 pp., Cambridge Univ. Press, New York, 1986.

Rossow, W. B., and L. C. Garder, Cloud detection using satellite measurements of infrared and visible radiances for ISCCP, *J. Clim., 6,* 2341-2369, 1993.

Saiedy, F., H. Jacobowitz, and D. Q. Wark, On cloud-top determination from Gemini-5, *J. Atmos. Sci., 24,* 63-69, 1967.

Sarkissian, A., H. K. Roscoe, and D. J. Fish, Ozone measurements by zenith-sky spectrometers: an evaluation of errors in air-mass factors calculated by radiative transfer models, *J. Quant. Spectrosc. Radat. Transfer, 54,* 471-480, 1995.

Saunders, R. W., and K. T. Kriebel, An improved method for detecting clear sky and cloudy radiances from AVHRR data, *Int. J. Remote Sens., 9,* 123-150, 1988.

Smith, W. L., and C. M. R. Platt, Comparison of satellite deduced cloud top heights with indications from radiosonde and ground-based laser measurements, *J. Appl. Meteorol., 17,* 1796-1802, 1978.

Stam, D. M., J. F. de Haan, J. W. Hovenier, and P. Stammes, Degree of linear polarization of light emerging from the cloudless atmosphere in the oxygen A-band, *J. Geophys. Res., 104,* 16,843-16,858, 1999.

Stammes, P., Errors in UV reflectivity and albedo calculations due to neglecting polarisation, *Proc. SPIE Int. Soc. Opt. Eng., 2311,* 227-235, 1994.

Stowe, L. L., C. G. Wellemeyer, T. F. Eck, H. Y. M. Yeh, and The NIMBUS-7 Data Processing Team, Nimbus-7 global cloud climatology, Part 1, Algorithms and validation, *J. Clim., 1,* 445-470, 1988.

Vanbauce, C., J. C. Buriez, F. Parol, B. Bonnel, G. Sèze, and P. Couvert, Apparent pressure derived from ADEOS-POLDER observations in the oxygen A-band over ocean, *Geophys. Res. Lett., 25,* 3159-3162, 1998.

Van de Hulst, H. C., *Multiple Light Scattering, Tables, Formulas, and Applications,* vols. 1 and 2, 739 pp., Academic, San Diego, Calif., 1980.

Winker, D. M., and C. R. Trepte, Laminar cirrus observed near the tropical tropopause by LITE, *Geophys. Res. Lett., 25,* 3351-3354, 1998.

Wu, M.-L. C., Remote sensing of cloud-top pressure using

reflected solar radiation in the oxygen A-band, *J. Climate and Appl. Meteorol., 24,* 593-546, 1985.

Yamamoto, G., and D. Q. Wark, Discussion of the letter by R. A. Hanel, 'Determination of cloud altitude from a satellite', *J. Geophys. Res., 66,* 3596, 1961.

Ziemke, J. R., S. Chandra, and P. K. Bhartia, Two new methods for deriving tropospheric column ozone from TOMS measurements: Assimilated UARS MLS/ HALOE and convective-cloud differential techniques, *J. Geophys. Res., 103,* 22,115-22,127, 1998.

J. F. de Haan and J. W. Hovenier, Department of Physics and Astronomy, Free University, De Boelelaan 1081, 1081 HV Amsterdam, Netherlands. (haandej@knmi.nl; hovenier@nat.vu.nl)

R. B. A. Koelemeijer and P. Stammes, Royal Netherlands Meteorological Institute, P.O. Box 201, 3730 AE De Bilt, Netherlands. (koelemei@knmi.nl; stammes@knmi.nl)

(Received May 17, 2000; revised July 26, 2000;
accepted October 10, 2000.)